Interannual Variability and Ensemble Forecast of Upper Blue Nile Basin Kiremt Season Precipitation

Paul Block[1] and Balaji Rajagopalan[1,2]

[1] Department of Civil Environmental and Architectural Engineering, University of Colorado Boulder, Colorado

[2] Co-operative Institute for Research in Environmental Sciences, University of Colorado, Boulder, Colorado

Abstract

Ethiopian agriculture and Nile River flows are heavily dependent upon the *Kiremt* season (June-September) precipitation in the upper Blue Nile basin, as a means of irrigation and streamflow contribution, respectively. Climate diagnostics suggest that the El Nino Southern Oscillation phenomenon is a main driver of interannual variability of seasonal precipitation in the basin. One-season (March-May) lead predictors of the seasonal precipitation are identified from the large-scale ocean-atmosphere-land system, including sea-level pressures, sea-surface temperatures, geopotential height, air temperature, and the Palmer Drought Severity Index. A nonparametric approach based on local polynomial regression is proposed for generating ensemble forecasts. The method is data-driven, easy to implement, and provides a flexible framework able to capture any arbitrary features (linear or nonlinear) present in the data, as compared to traditional linear regression. The best subset of predictors, as determined by the Generalized Cross Validation (GCV) criteria, is selected from the suite of potential large-scale predictors. A simple technique for disaggregating the seasonal precipitation forecasts into monthly forecasts is also provided. Cross-validated forecasts indicate significant skill in comparison to climatological forecasts, as currently utilized by the Ethiopian National Meteorological Services Agency. This ensemble forecasting framework can serve as a useful tool for water resources planning and management within the basin.

1. Introduction

Ethiopia is predominantly an agronomic society, and the success of seasonal crops has large implications, ranging from the state of the countrywide economy to the survival of the subsistence farmer. As the vast majority of agriculture is rain-fed, precipitation plays a pivotal role in the country's welfare. Roughly 70 percent of annual precipitation in the upper Blue Nile basin of Ethiopia is delivered during the *Kiremt* season, composed of the June-September months (Conway, 2000); during this season, 85-95 percent of annual crops are produced (Degefu, 1987). Precipitation also plays another equally important role in the Ethiopian highlands, feeding the headwaters of the Blue Nile (shown in Figure 1) and Atbara Rivers, which eventually supply the mighty Nile River. Runoff in these basins contributes almost 70 percent of the annual Nile flow into Egypt, with the vast majority occurring during the *Kiremt* season (Yates and Strzepek, 1998). Policy and planning tools, including water management, economic, hydropower, and irrigation models for Ethiopia and other downstream countries, rely heavily on precipitation and streamflow as key parameters.

Therefore, understanding and predicting the year-to-year variability of the seasonal rainfall is of immense importance in mitigating potential disasters. Presently, the Ethiopian National Meteorological Services Agency relies solely on climatology and persistence in forecasting seasonal precipitation (Gissila et al., 2004). This motivates the current research to develop a robust framework for generating ensemble forecasts of the *Kiremt* season precipitation.

This paper begins with a description of the data sets utilized, followed by background on Ethiopian climatology and interannual variability. Potential predictors of

the seasonal precipitation are then identified. Next, the proposed nonparametric approach for producing ensemble forecasts is presented, along with the traditional linear regression method. Skill evaluation methods are subsequently described, followed by the results of the *Kiremt* seasonal precipitation forecast. The paper concludes with a summary and discussion of the results.

2. Data Description

Precipitation

The precipitation data utilized for this study is part of the CRU TS 2.0 dataset, obtained from the University of East Anglia, available at http://www.cru.uea.uk/~timm/grid/CRU_TS_2_0.html. It consists of monthly rainfall data on a 0.5^{o} x 0.5^{o} grid for the period 1901-2000. However, much of the data from 1901-1960 is synthetic, and is obtained based on 1961-1990 averages and gridded anomalies. This study, therefore, includes only 1961-2000, minimizing the synthetic data and reducing the likelihood of unwanted trends or potential persistence in the data. Additionally, since this study focuses on the *Kiremt* season, only the seasonal total for the June-September data are retained for each year. The upper Blue Nile basin within Ethiopia constitutes 68 grid points.

As a result of the sparse and spotty precipitation gauges in the region, the upper Blue Nile basin precipitation data from the CRU set (1961-2000) was validated to ensure its spatial and temporal representation. This was accomplished by comparison with two other global precipitation datasets: University of Delaware, a 0.5^{o} x 0.5^{o} gridded set of monthly precipitation values for the period 1950-1999, and the Climate Prediction

Center's merged analysis precipitation (CMAP) data, a 2.5^o x 2.5^o gridded set of monthly precipitation for 1979 to the present.

The CRU and University of Delaware data are highly correlated over the upper Blue Nile basin, exhibiting a correlation coefficient of 0.79 for the average *Kiremt* season precipitation. This suggests that the two data sets are consistent. In correlating the aerial average *Kiremt* season precipitation from CRU with the gridded CMAP data (Figure 2), high correlations over the region were again found. These validations appear to certify the consistency of the CRU set. To demonstrate the spatial homogeneity of the precipitation, a principal component analysis (von Storch and Zwiers, 1999) of seasonal precipitation at the 68 grid locations in the region was performed. The first leading pattern captures approximately 58 percent of the spatial data variance. The first spatial pattern (Figure 3) shows similar magnitude and sign across the region, indicating that the leading pattern of variability is spatially homogenous, confirming results from earlier studies (Eklundh and Pilesjo, 1990). Furthermore, the first temporal pattern (i.e. principal component) is highly correlated (correlation coefficient of 0.98) with the aerial average seasonal precipitation (Figure 4). As a result, the aerial average *Kiremt* season precipitation may be considered as an excellent representative of the seasonal rainfall in the upper Blue Nile basin, henceforth, referred to as the UBN.

Large-scale Climate Variables

Global atmospheric and oceanic variables including, sea-surface temperature (SST), sea-level pressure (SLP), geopotential height, air temperature, and outgoing long-wave radiation (OLR), were obtained from the National Oceanic and Atmospheric

Administration's (NOAA) climate diagnostics center (CDC) (http://www.cdc.noaa.gov), based on NCEP/NCAR re-analysis data (Kalnay et al., 1996). These are monthly average values on a 2.5^{o} x 2.5^{o} grid for 1949 to the present. Palmer Drought Severity Index (PDSI) values (Dai et al., 2004), also at monthly time scales and on a 2.5^{o} x 2.5^{o} grid, for 1870-2003, were provided by the National Center for Atmospheric Research's Climate and Global Dynamics Division (http://www.cgd.ucar.edu/cas/catalog/climind/pdsi.html.)

3. Large-scale climate and *Kiremt* season precipitation

Two main rainy seasons exist within Ethiopia: the *Belg* ("small rains") and the *Kiremt* ("big rains"). The *Kiremt* season is part of a larger east African monsoon season spurred on by the shifting of the Intertropical Convergence Zone (ITCZ) northward (Griffiths, 1972; Gamachu, 1977). During the pre-monsoon season (March-May) the central African land is predominantly dry, resulting in a general warming of the regional land and atmosphere. This solar heating and warming of the surface creates a low pressure, and pulls the ITCZ to the north from the equatorial region. Figures 5 and 6 illustrate this basic climatology. Figure 5 presents PDSI and air temperatures patterns during the pre-monsoon season, indicating a dry and warm band spanning central Africa near 10-15 degrees north. Figure 6 presents wind patterns during the pre-monsoon and monsoon season; the change in wind direction consistent with the ITCZ movement and warming of the Indian Ocean is evident. The extent to which the ITCZ reaches is the dominant factor in controlling the timeliness and quantity of *Kiremt* rains. Simultaneous to the shifting of the ITCZ, high-pressure systems in the South Atlantic and Indian Oceans, coupled with the Arabian and the Sudan thermal lows, allow for the influx of

moisture (NMSA, 1996; Seleshi and Zanke, 2004). While the tropical easterly and Somali jets deliver precipitation to the eastern edge of the country due to the land-ocean gradient, the highlands and Blue Nile basin are predominantly fed by moisture advected over the Congo basin, transported via a southwesterly flow, and released due to orographic effects (see Figure 6b). This pattern persists until September or October, when the jet stream in northeast Africa is reestablished, and the ITCZ shifts south.

Interannual variability of precipitation within the upper Blue Nile basin has been investigated by previous researchers (see e.g., Eklundh and Pilesjo, 1990; Seleshi and Demaree, 1995; Camberlin, 1995; Osman and Sauerborn, 2002; Conway, 2000). Factors influencing the variability include the El Niño Southern Oscillation (ENSO) phenomenon, tropical depressions over the Indian Ocean, and periods of anomalous warming over the Indian Ocean. Correlations of UBN boreal summer rains with ENSO have shown that warm ENSO periods (El Niño years) are typically associated with lower precipitation and drought years, while cold periods (La Nina years) are associated with higher precipitation quantities (Seleshi and Zanke, 2004; Ntale and Gan, 2004; Nicholson and Kim, 1997; Beltrando and Camberlin, 1993). During warm ENSO events, the full migration of the ITCZ northward is inhibited, as the land and atmosphere have not sufficiently warmed to continue to draw the ITCZ to its full potential. This occurrence blocks moist air from the south and moisture produced due to the convective nature of the ITCZ, often resulting in drought circumstances. Along a separate vein, the *Kiremt* season rains in Ethiopia and pressure anomalies in Bombay, India, independent of ENSO, have also been found to be significantly correlated (Camberlin, 1995 and 1997).

A correlation map between the first principal component of UBN rainfall and simultaneous global sea-surface temperatures is shown in Figure 7. The ENSO pattern is quite clear in the Pacific Ocean corroborating earlier studies, and giving further credence to ENSO being the leading factor of variability for the *Kiremt* season precipitation. Figure 7 also indicates regions of correlation in the Atlantic, which are well known to affect Sahelian precipitation (Palmer, 1986; Druyan and Koster, 1989; Cook, 1997), and may warrant further attention. The realization that the ENSO phenomenon is one of the main drivers of seasonal rainfall in the region, and is both persistent and predictable, offers promise for improved forecasts of *Kiremt* season precipitation.

The effects of climate change on precipitation in the highlands of Ethiopia, as well as the whole of the Nile basin, have also been given attention recently. While precipitation quantities and number of rainy days in most parts of Ethiopia have declined significantly since 1982, Seleshi and Zanke (2004) have found that no such trends are evident for the Ethiopian highlands during the period 1965-2002. Potential climate change effects are not explicitly dealt with in this study, but merit further investigation.

4. Identification of Predictors

Given the strong ENSO teleconnection that previous studies and this analysis (Figure 7) have identified with the UBN rainfall, a logical first step is to correlate UBN rainfall with standard ENSO indices of the preceding season (Table 1). The table reveals some significant, yet relatively weak, correlations with the pre-monsoon ENSO indices. To identify potentially stronger predictors, the seasonal precipitation was correlated with large-scale ocean-atmosphere-land variables from the preceding season. This approach

for identification of predictors was used by Grantz et al. (2005) and Singhrattna et al. (2005) for skillful forecast of spring streamflow in the Truckee basin in the western USA and Thailand rainfall, respectively. Figures 8 and 9 illustrate correlation maps of UBN rainfall with global SST and SLP, respectively. The correlation patterns in these two figures again resemble ENSO features and are therefore consistent with the teleconnection identified previously. Specific regions that exhibit substantial positive or negative correlations are indicated by circled sections. The SST and SLP from the regions of high correlation are averaged over the region to form predictors. Additionally, to further enhance the correlation, SST and SLP indices were created by subtracting the negatively correlated region from the positively correlated one. Correlations with other variables, such as 500mb geopotential heights, OLR, air temperature and PDSI were also performed to capture regional aspects. A negative correlation with geopotential height was noted off the southwestern coast of Africa, which is associated with the St. Helena high pressure system that influences wind flow patterns routed toward Ethiopia (see Figure 3). The OLR also has regional influences effecting *Kiremt* season rains and acts as a proxy for the thermal conditions of the land and ocean, a key constituent in establishing African monsoon conditions. The correlation map of OLR with seasonal precipitation (not shown) registered a strong negatively correlated region southwest of Somalia, in the Indian Ocean. The preferred variable for the land-ocean thermal gradient and ITCZ migration extent would be soil moisture, but this data is non existent, so PDSI is utilized as a reasonable surrogate (Simms et al., 2002; Guttman et al., 1992). A region covering the northern part of Ethiopia, just north of the basin, exhibited significant positive correlation during the pre-monsoon season with the UBN precipitation, and was

selected as a potential predictor. Similarly, regions of high correlation with surface temperature were identified for potential inclusion (see Figure 10), and an air temperature index created. All of these variables capture the important and varying features of the summer rainfall in the basin. The culmination of this effort was the identification of a suite of predictors of UBN rainfall, denoted in Table 2.

5. Forecasting Framework

Previous studies have developed linear regression based forecast models for precipitation within Ethiopia (Gissila et al., 2004; Eklundh and Pilesjo, 1990; Haile, 1987) but not specifically for the upper Blue Nile basin. Gissila et al. grouped Ethiopia into four clusters and developed a linear regression model based on nine SST related predictors. Eklundh and Pilesjo spatially divided Ethiopia into seven regions by a principal component analysis and created corresponding linear regression models based on elevation, latitude, and longitude. Linear regression models based on large-scale climate predictors and a principal component analysis of predictors in Ethiopia and surrounding countries have also been created for prediction of Nile River flows (Eldaw et al., 2003). These forecasting efforts serve as a good starting point, but suffer from two main drawbacks. First, with limited data length and multicollinearity (i.e. correlations between predictors), skill scores may be artificially high; no apparent efforts were made in the above studies to address this issue. Secondly, in a linear regression framework nonlinear relationships cannot be captured.

The motivation in this paper is to provide a robust and flexible framework that alleviates these drawbacks. To this end, a nonparametric modeling approach based on a local polynomial method is offered.

Generally, regression models take the simple form

$$Y = f(\mathbf{x}) + e \qquad (1)$$

where **x** represents a vector of predictors, f is the function, Y the dependent variable and e is the error, often assumed to be normally distributed with a mean of zero and variance σ^2. Traditional linear regression involves fitting a linear function f to the entire data. If there are 'p' predictors then the linear regression model, expanding Equation *(1)*, takes the form:

$$y_t = \beta_0 + \beta_1 x_{1t} + \beta_2 x_{2t} + \ldots + \beta_p x_{pt} + e_t \qquad t = 1 \text{ to } N \qquad (2)$$

where y_t is the response variable (seasonal precipitation in this paper), $x_1, \ldots, x_p$ are the predictor variables, $\beta_o, \ldots, \beta_p$ are the regression coefficients, e_t refers to the model error (difference between observed and estimated values), and N is the total number of observations. The coefficients are estimated by minimizing the sum of squares of the errors (also known as the ordinary least squares method). Key assumptions of this traditional approach include normal distribution of the variables (or transformation to a normal distribution), and uncorrelated and normally distributed errors with a mean of zero. Upon fitting the coefficients, estimation (or prediction) at a new point, y_{pred}, for a new predictor vector $\boldsymbol{x}_{pred}$ is obtained from the above equation. Along with y_{pred}, the standard deviation of the predictive error, σ_{pe}, may also be obtained from theory (Helsel and Hirsch, 1995). Normal random deviates with mean zero and variance σ^2_{pe} when added to y_{pred}, provide an ensemble forecast.

Linear regression approaches are widely used due to well developed theory and readily available software. However, the methodology has several drawbacks: (i) the assumption of normality of variables, even through transformations, is often difficult to satisfy, (ii) regression coefficients are greatly influenced by a small number of outliers, often leading to a poor fit, (iii) nonlinear relationships between the dependent and independent variables cannot be captured, and (iv) if the linear model does not provide a good fit, few choices of higher order models exist, especially considering short dataset lengths.

Local Polynomial Regression Model

Nonparametric methods provide an attractive alternative for addressing the drawbacks of traditional linear regression. In the nonparametric approach, estimation of the function f is performed 'locally' at the point to be estimated. This 'local' estimation provides the ability to capture features (i.e. nonlinearities) that might be present locally, without granting outliers any undue influence in the overall fit. Several nonparametric methods for regression and probability density function estimation exist; for an overview of these methods and their applications to hydroclimatology, see Lall, 1995.

In this work, the local polynomial based nonparametric approach (Loader, 1999) is proposed for its ease in understanding, implementation and successful past applications. The methodology is described in the following algorithm. (Subscript p represents 'predictive', and l represents 'local').

For a point of interest where an estimation of the function is desired, say $\boldsymbol{x}_{pl}$:

(i) K (= αN) nearest neighbors are identified in proximity to $\boldsymbol{x}_{pl}$. The neighbors can be obtained using either the Euclidean or Mahalanobis distance. The parameter α describes the size of the neighborhood and is within the (0,1] range. Clearly, if α takes a value of 1, the number of neighbors selected includes all data points.

(ii) A polynomial of order P is fit to the K nearest neighbors, using a weighted least squares method. The fitted polynomial is used to obtain the estimate of the dependent variable, y_{pl}. The 'local' error standard deviation, σ_{pl}, can be obtained from regression theory.

(iii) The K residuals from the fitted polynomial in (ii) can be re-sampled (Prairie et al., 2005; Grantz et al., 2005) or bootstrapped and added to y_{pl} to create an ensemble. Alternatively, random deviates from a normal distribution with mean zero and standard deviation of σ_{pl} can be generated and added to y_{pl} to create an ensemble. The later technique is implemented in this study.

$\boldsymbol{x}_{pl}$ may be an observed data point or a new point. It is noteworthy to mention that for α=1 and P=1, this approach collapses to the traditional linear regression, thus making it a more general and flexible approach.

The optimal values of the two parameters K (or α) and P must be estimated from the data, and may be obtained using the Generalized Cross Validation (GCV) score function, given as:

$$GCV(\alpha, P) = \frac{\sum_{t=1}^{N} \frac{e_t^2}{N}}{\left(1 - \frac{m}{N}\right)^2} \qquad (3)$$

where e_t is the model residual (difference between observed and model estimated values of the dependent variable), m the number of predictors in the fitted polynomial, and N the number of data points. The GCV function penalizes over-fitting (large numbers of predictors) and is a very good estimate of the predictive risk (Craven and Wahba, 1979).

For each combination of α and P, the model is fit, as described in the algorithm above, and the GCV score computed; the combination providing the minimum GCV score is selected as the optimal one.

The GCV function can also be used to select the best subset from a suite of predictors. This process involves including different combinations of predictors, along with varying α and P values, calculating the GCV, and selecting the combination of predictors, α, and P that provide the minimum GCV score as the best parameter combination. The use of GCV for predictor subset selection is fairly recent (Regonda et al., 2005a; Regonda et al., 2005b) and has been shown to be quite effective. GCV may also be used for predictor selection in a linear regression framework, in lieu of the common stepwise regression approach (Rao and Toutenburg, 1999; Walpole et al., 2002). Typically, the best subset of predictors selected by the GCV function contains no multicollinearities, but occasionally some remain, in which case one of the predictors is eliminated from the subset (Regonda et al., 2005a; Regonda et al., 2005b). One means of eliminating multicollinearity entirely is to perform a principal component analysis on the predictor set and use the principal components (which are orthogonal by construction) in the subset selection.

For the UBN seasonal rainfall with eight potential predictors from Tables 1 and 2, the GCV score function led to the optimal parameter values of α and P equal to one, and

a best subset of five predictors (indicated as bold in Table 2) comprising sea-level pressure index, sea-surface temperature index, geopotential height, air temperature index, and PDSI.

6. Model Validation

The forecasts are validated in a cross-validation mode, in which data from a given year is dropped and an ensemble forecast is issued by the model fit on the remaining data points. This is repeated for all 40 years (1961-2000), mimicking a prediction-type assessment. Ideally, α and P would be checked and modified for each year in the cross-validation mode, but dropping one year at a time proved to have little influence, so the parameters were held at 1, their optimal values based on the GCV for all years.

The cross-validated ensemble forecasts are evaluated by two measures: (i) correlation coefficients between the median of the ensembles and the observed values, and (ii) Rank Probability Skill Scores (RPSS).

The RPSS (Wilks, 1995), a measure of the skill of ensemble forecasts, is a widely used probabilistic measure for comparison with prediction by climatology forecasts. The general form of the rank probability score (RPS) equation for any year takes the form:

$$RPS = \sum_{m=1}^{R} (CP_{F,m} - CP_{O,m})^2 \qquad (4)$$

where R is the number of categories, $CP_{F,m}$ is the cumulative predicted probability for the forecast ensemble (through category m), and $CP_{O,m}$ is the cumulative observed probability (also through category m). This study incorporates three categories of equal size, such that the climatological probability of being in each category is 1/3; for the

category that was observed the probability is one, and zero elsewhere. A perfect forecast results in RPS equaling zero. The RPSS is then defined as:

$$RPSS = 1 - \frac{RPS_{FORECAST}}{RPS_{CLIMATOLOGY}} \qquad (5)$$

RPSS values range from +1 to -∞. A value of +1 represents perfect skill, or a perfect forecast, while negative values represent poor skill; any value above zero represents an improved forecast over climatology. The RPSS is calculated for each year separately.

7. Results

Using the best set of predictors, cross-validated ensemble predictions of the *Kiremt* season UBN rainfall were generated from the local polynomial and linear regression forecast models, shown in Figures 11 and 12, respectively. The ensembles of each year are shown as box plots in the figures, with the box covering the 25th and 75th percentile, the horizontal line inside the box representing the median, and whiskers extending to the 5th and 95th percentile of the ensembles. Dotted horizontal lines are also included for the 5th, 25th, 50th, 75th, and 95th percentiles from the observed record. The correlation between the median value of the ensemble prediction and the observed values are quite strong, at 0.67 and 0.69 for the local polynomial and linear approaches, respectively; however, the median RPSS for the 1961-2000 period are 0.39 and 0.25, respectively. This suggests that on average, the local polynomial approach outperforms the linear regression approach. The RPSS for the extreme wettest and driest years (ten each) from the local polynomial approach is 0.86 and 0.94, respectively, indicating that the ensemble forecast framework provides skilful ensemble forecasts in the extreme years, which are of great consequence in resource planning and management.

The relationships between UBN rainfall and the predictors are largely linear, evident by optimal values of α and P equal to one, and similar skill scores between the two approaches. However, subtle nonlinearities exist, apparent in Figure 13, which illustrates the relationship between the seasonal precipitation and two leading predictors: SST and SLP. It is the capability of the local polynomial approach to capture such subtle features that makes it so attractive.

The ensembles also provide the forecast of the Probability Density Functions (PDF). Figure 14 demonstrates PDF from the nonparametric ensembles (dashed line) and from the observed data (i.e. climatological PDF, solid line) for two wet years (1978 and 1982) and two dry years (1968 and 1974). The observed UBN precipitation value for the year is indicated by the dotted vertical line. The PDF are estimated using a nonparametric kernel density estimator (Bowman and Azzalini, 1997). For the wet years, the PDF from the forecast ensembles are shifted to the right of the climatological PDF, indicative of increased precipitation. The observed value in 1968 is in the center of the ensemble PDF, indicating an excellent fit, while in 1974 the rightward shift is clear but not perfect, as the observed value was relatively extreme. Inspection of the dry years leads to similar findings, as the PDF are shifted to the left of the climatological PDF, indicative of drier conditions.

The ensembles and PDF provide a structure in which threshold exceedance probabilities may be obtained. For demonstration, thresholds were selected at 1070mm (90^{th} percentile) and 805mm (10^{th} percentile) to represent flood and drought conditions, respectively. This implies that climatologically, there is a 10% chance in any given year of having a flood or an equal chance of experiencing a drought. By visual inspection,

Figure 14 clearly improves upon this prediction. Table 3 presents the exceedance (for floods) and non-exceedance (for droughts) probabilities, which show considerably higher probabilities than climatology. Note that seasonal precipitation for 1964, 1974, 1982 and 1987 are outside their respective threshold limits, while 1968 and 1978 are not. 1964 and 1987 are the wettest and driest seasons in the 1961-2000 record.

Such exceedance probability forecasts, if provided in advance of the *Kiremt* season to water managers and decision-makers within the basin, is of tremendous value. It allows them to make educated judgments about reservoir operation, crop irrigation, conservation measures (droughts), potential emergency response measures (floods), or a number of other critical aspects. Additionally, the value of ensemble forecasts also becomes evident for use in streamflow or water balance models, to describe the reaction of these systems from a probabilistic standpoint.

Although the skill scores of the seasonal model are good, numerous process models within the basin (e.g., water balance, economic, crop) require monthly inputs. One methodology to accomplish this involves applying the framework developed here for each month and obtaining an ensemble forecast for each month separately. This can be computationally intensive and furthermore, the generated monthly ensemble forecasts might not capture the dependence between months. A better approach is to disaggregate the seasonal forecast into monthly values. To achieve this, K nearest neighbors to the seasonal forecast value, y_{pred}, are identified (i.e., historical years that have a similar seasonal precipitation magnitude as the forecast value). A probability metric is created by providing maximum weight to the nearest neighbor and least weight to the farthest neighbor (Lall and Sharma, 1996), as shown in the following equation:

$$W(j) = \frac{1/j}{\sum_{j=1}^{K} 1/j} \qquad (6)$$

Using the metric, one of the K nearest neighbor is selected, say year J. The monthly fractions of the seasonal precipitation in year J (proportion vector) are then multiplied by y_{pred} to obtain the monthly disaggregated values. Since the historical monthly fractions must sum to one, the disaggregated values must also sum to the seasonal forecast values. Repeating this for each ensemble forecast provides an ensemble of monthly forecasts.

As a demonstration, Figure 15 illustrates box plots of the ensembles for each month of the 1975 *Kiremt* season, disaggregated using the method described above, with observed monthly values shown as dots. The simulations capture the observed values quite well. This technique is fairly rudimentary and easy to implement, but detailed validation is still required; these processes are underway. Improved nonparametric disaggregation techniques (Prairie et al., 2005) can also be used to fully capture the correlation between the months.

8. Summary and Discussion

A framework is proposed for ensemble forecast of *Kiremt* season (June-September) precipitation for the upper Blue Nile basin within Ethiopia. A suite of predictors from the land-ocean-atmosphere system are identified that capture various aspects of the summer rainfall, including movement of the ITCZ and the large-scale ENSO teleconnections. A nonparametric approach based on local polynomial regression is adapted for generating ensemble forecasts. This also includes use of the GCV function for selecting the best subset (five) of predictors out of a suite of eight potential predictors.

The ensemble forecasts are generated for each year in a cross-validated mode and skills evaluated using the RPSS probabilistic skill score measure. The forecast ensembles demonstrate significant overall skill and very high skills during extreme wet and dry years compared to climatological forecast utilized by the Ethiopian National Meteorological Services Agency. A simple nonparametric method for disaggregating the seasonal forecasts to monthly values was also outlined.

The nonparametric framework offers a flexible and attractive alternative to traditional linear regression. The 'local' estimation method possesses the ability to capture any arbitrary relationship structure present in the data, without being required to satisfy normality of the variables or being overly influenced by a small number of outliers.

The use of the GCV function for predictor selection is noteworthy. While it is robust, several combinations of predictors provide similarly low GCV scores. To alleviate potential ambiguity between similar models, a multi-model ensemble forecast approach could be adopted (Regonda et al., 2005a,b), in which the top few predictor sets (and corresponding models) are retained. Forecast ensembles are then generated from the suite of models with similar GCV scores and optimally combined by a weighting scheme. This methodology may help to generally improve forecast skill, specifically by dampening poor forecasts (1962, 1989, and 1992).

Other aspects also warrant attention for further study. To ensure that multicollinearities between predictors have been entirely eliminated, a principal component analysis on the suite of predictors could be performed, with the ensuing principal components used as new predictors in the subset selection. Along another vein,

cross-validated ensemble forecasts could be generated by means of dropping a set of years, as opposed to only one year, and assessed with the skill score measures. This approach may prove insightful for predictive capabilities on a reduced dataset.

Acknowledgements

This research study was partially funded by a grant from the U.S. Agency for International Development (USAID) through the International Food Policy Research Institute (IFPRI), and forms part of the first author's Ph.D. dissertation at the University of Colorado – Boulder.

References

Beltrando, G., P. Camberlin, 1993: Interannual variability of rainfall in the eastern Horn of Africa and indicators of atmospheric circulations. *International Journal of Climatology* **13**, 533-546.

Bowman, A., and A. Azzalini, 1997: *Applied smoothing techniques for data analysis*. Oxford University Press, New York.

Camberlin, P., 1995: June-September rainfall in north-eastern Africa and atmospheric signals over the tropics: A zonal perspective. *International Journal of Climatology* **15**, 773-783.

Camberlin, P., 1997: Rainfall anomalies in the source region of the Nile and their connection with Indian summer monsoon. *Journal of Climate* **10**, 1380-1392.

Clark M., L. Hay, 2004: Use of medium-range numerical weather prediction model output to produce forecasts of streamflow. *Journal of Hydrometeorology* **5**, 15–32.

Conover, W., 1971: *Practical nonparametric statistics*. New York: John Wiley & Sons.

Conway, D., 2000: The climate and hydrology of the Upper Blue Nile, Ethiopia. *Geographical Journal* **166**, 49-62.

Cook, K., 1997: Large-Scale Atmospheric Dynamics and Sahelian Precipitation. *Journal of Climate* **10**, 1137-1152.

Craven, P., and G. Wahba, 1979: Smoothing noisy data with spline functions. *Journal of Numerical Mathematics* **31**, 377-403.

Dai, A., K. Trenberth, and T. Qian, 2004: A global data set of Palmer Drought Severity Index for 1870-2002: Relationship with soil moisture and effects of surface warming. *Journal of Hydrometeorology* **5**, 1117-1130.

Degefu, W., 1987: Some aspects of meteorological droughts in Ethiopia. *Drought and Hunger in Africa*. Glantz MH (ed.) Cambridge University Press.

Druyan, L., and R. Koster, 1989: Sources of Sahel precipitation for simulated drought and rainy seasons. *Journal of Climate* **2,** 1438-1446.

Eklundh, L., P. Pilesjo, 1990: Regionalization and spatial estimation of Ethiopian mean annual rainfall. *International Journal of Climatology* **10,** 473-494.

Eldaw, A., J. Salas, L. Garcia, 2003: Long-range forecasting of the Nile River flows using climatic forcing. *Journal of Applied Meteorology* **42,** 890-904.

Gamachu, D., 1977: *Aspects of climate and water budget in Ethiopia*. Addis Ababa University Press: Addis Ababa.

Gissila, T., E. Black, D. Grimes, J. Slingo, 2004: Seasonal forecasting of the Ethiopian summer rains. *International Journal of Climatology* **24**, 1345-1358.

Grantz, K., 2003: *Using large-scale climate information to forecast seasonal streamflows in the Truckee and Carson rivers*. Master of Science thesis, University of Colorado, Boulder, CO.

Grantz, K., B. Rajagopalan, M. Clark and E. Zagona, 2005: Seasonal Shifts in the North American Monsoon, (in review) *Journal of Climate*.

Griffiths, J., 1972: *Ethiopian Highlands. World Survey of Climatology*, Landsberg H (ed.). Climates of Africa, vol. 10. Elsevier: Amsterdam, 369-388.

Guttman, N., J. Wallis, and J. Hosking, 1992: Spatial Comparability of the Palmer Drought Severity Index, *Water Resources Bulletin* **28,** 1111- 1119.

Haile, T., 1987: A case study of seasonal forecasting in Ethiopia. *WMO regional association I*. Geneva, Switzerland, 53-76.

Helsel, D., R. Hirsch, 1995: *Statistical methods in water resources*. Elsevier Science: Amsterdam.

Kalnay, E., M. Kanamitsu, R. Kistler, W. Collins, D. Deaven, L. Gandin, M. Iredell, S.Saha, G. White, J. Woollen, Y. Zhu, M. Chelliah, W. Ebisuzaki, W. Higgins, J.Janowiak, K. C. Mo, C. Ropelewski, J. Wang, A. Leetmaa, R. Reynolds, R. Jenne, and D. Joseph, 1996: The NCEP/NCAR reanalysis 40-year project. *Bulletin of the American Meteorology Society* **77**, 437-471.

Lall, U., 1995: Recent advances in nonparametric function estimation: Hydraulic applications. *Reviews of Geophysics* **33,** 1093-1102.

Lall, U., and A. Sharma, 1996: A nearest neighbor bootstrap for resampling hydrologic time series, *Water Resources Research*, **32,** 679-693.

Loader, C., 1999: *Local Regression Likelihood*. Springer: New York.

Mitchell, T., P. Jones, 2005: An improved method of constructing a database of monthly climate observations and associated high-resolution grids. *International Journal of Climatology* **25,** 693:712.

Nicholson, S., J. Kim, 1997: The relationship of the El Niño-Southern Oscillation to the African rainfall. *International Journal of Climatology* **17,** 117-135.

Ntale, H., T. Gan, 2004: East African rainfall anomaly patterns in association with El Niño/Southern Oscillation. *Journal of Hydrologic Engineering* **9**, 257-268.

NMSA, 1996: *Climate and agroclimate resources of Ethiopia*. NMSA Meteorological Research Report Series, vol. 1, No. 1, Addis Ababa.

Osman, M., P. Sauerborn, 2002: A preliminary assessment of characteristics and long-term variability of rainfall in Ethiopia – basis for sustainable land use and resource management. *Conference in International Agriculture Research, Deutscher Tropentag*, Witzenhausen, 9-11 October.

Palmer, T., 1986: Influence of the Atlantic, Pacific, and Indian Oceans on Sahel rainfall. *Nature* **322**, 251-253.

Prairie, J., B. Rajagopalan, U. Lall and T. Fulp, 2005: A Stochastic Nonparametric Technique for Space-Time Disaggregation of Streamflows (in review) *Water Resources Research*.

Regonda, S., B. Rajagopalan, U. Lall, M. Clark and Y. Moon, 2005a: Local polynomial method for ensemble forecast of time series, *Nonlinear Processes in Geophysics,* Special issue on "Nonlinear Deterministic Dynamics in Hydrologic Systems: Present Activities and Future Challenges" **12**, 397-406.

Regonda, S., B. Rajagopalan, M. Clark and E. Zagona, 2005b: Multi-model Ensemble Forecast of Spring Seasonal Flows in the Gunnison River Basin (in review) *Water Resources Research*.

Rajagopalan, B., K. Grantz, S. Regonda, M. Clark and E. Zagona, 2005: *Ensemble streamflow forecasting: Methods and Applications.* Advances in Water Science Methodologies, Ed by U. Aswathanarayana, Taylor and Francis, Netherlands.

Rao, C., and H. Toutenburg, 1999: *Linear Models: Least Squares and Alternatives*. Springer, New York.

Sankarasubramanian A., U. Lall, 2003: Flood quantiles in a changing climate: Seasonal forecasts and causal relations. *Water Resources Research* **39**, 1134.

Saunders, M., and C. Fletcher, 2004: *Verification of Spring 2004 UK City Temperature Seasonal Forecasts*. Department of Space and Climate Physics, University College, London, UK.

Seleshi, Y., G. Demaree, 1995: Rainfall variability in the Ethiopian and Eritrean highlands and its link with the Southern Oscillation index. *Journal of Biogeography* **22**, 945-952.

Seleshi, Y., U. Zanke, 2004: Recent changes in rainfall and rainy days in Ethiopia. *International Journal of Climatology* **24**, 973-983.

Shahin, M., 1985: *Hydrology of the Nile Basin*, Elsevier, Amsterdam.

Sims, A., D.S. Niyogi, and S. Raman, 2002: Adopting drought indices for estimating soil moisture: A North Carolina case study. *Geophysical Research Letters* **29**, 1183.

Singhrattna, N., B. Rajagopalan, M. Clark and K. Krishna Kumar, 2005: Forecasting Thailand summer monsoon rainfall. *International Journal of Climatology* **25**, 649-664.

Souza, F., U. Lall, 2003: Seasonal to interannual ensemble streamflow forecast for Ceara, Brazil: applications of a multivariate, semi-parametric algorithm. *Water Resources Research* **39**, 1307-1320.

Von Storch, H., and F. W. Zwiers, 1999: *Statistical Analysis in Climate Research*. Cambridge Univ. Press, Cambridge.

Walpole, R., R. Myers, S. Myers, K. Ye, and K. Yee, 2002: *Probability and Statistics for Engineers and Scientists*. Prentice Hall, Upper Saddle River, New Jersey.

Wilks, D., 1995: *Statistical methods in atmospheric science: An Introduction*. Academic Press: San Diego.

Willmott, C., K. Matsuura, 2001: *Terrestrial air temperature and precipitation: monthly and annual time series (1950-1999)*. Center for Climatic Research, Department of Geography, University of Delaware, Newark, DE.

Yates, D., K. Strzepek, 1998: Modeling the Nile basin under climate change. *Journal of Hydrologic Engineering* **3**, 98-108.

Figure Captions

Figure 1: The Upper Blue Nile Basin, Ethiopia

Figure 2: Correlation of CRU and CMAP precipitation data

Figure 3: Contours of the first empirical orthogonal function of *Kiremt* precipitation data

Figure 4: *Kiremt* season precipitation and PC1 anomaly time-series

Figure 5: May Palmer Drought Severity Index (a) and March-May Air Temperature (b)

Figure 6: African wind patterns during the March-May (a) and *Kiremt* (b) seasons

Figure 7: Correlation map of the first principal component of UBN summer precipitation and global sea-surface temperatures (shaded region represents 90% significance level)

Figure 8: Correlation map of UBN summer precipitation with March-May sea-surface temperatures (shaded regions represent 90% significance level)

Figure 9: Same as Figure 8 but with sea-level pressures

Figure 10: Same as Figure 8 but with air temperature

Figure 11: Local polynomial modeling approach forecast results. Observed data shown as solid line; cross-validated model estimates shown as dashed line and boxes

(a) observed and cross-validated estimates ($R^2 = +0.67$) with horizontal lines at percentiles from the observed seasonal precipitation

(b) box plots of cross-validated ensembles(RPSS median = 0.39) with horizontal lines at percentiles from the observed seasonal precipitation

Figure 12: Linear modeling approach forecast results. Observed data shown as solid line; cross-validated model estimates shown as dashed line and boxes

(a) observed and cross-validated estimates ($R^2 = +0.69$) with horizontal lines at percentiles from the observed seasonal precipitation

(b) box plots of cross-validated ensembles(RPSS median = 0.25) with horizontal lines at percentiles from the observed seasonal precipitation

Figure 13: Surface plot of *Kiremt* season precipitation as a function of SST and SLP predictors.

Figure 14: PDF for wet (top) and dry (bottom) years. Climatological PDF shown as solid line; ensemble forecast PDF shown as dashed line. The observed precipitation is shown as a dotted vertical line.

Figure 15: Box plots of disaggregated monthly forecasts of *Kiremt* seasonal ensemble forecast for 1975

Figures

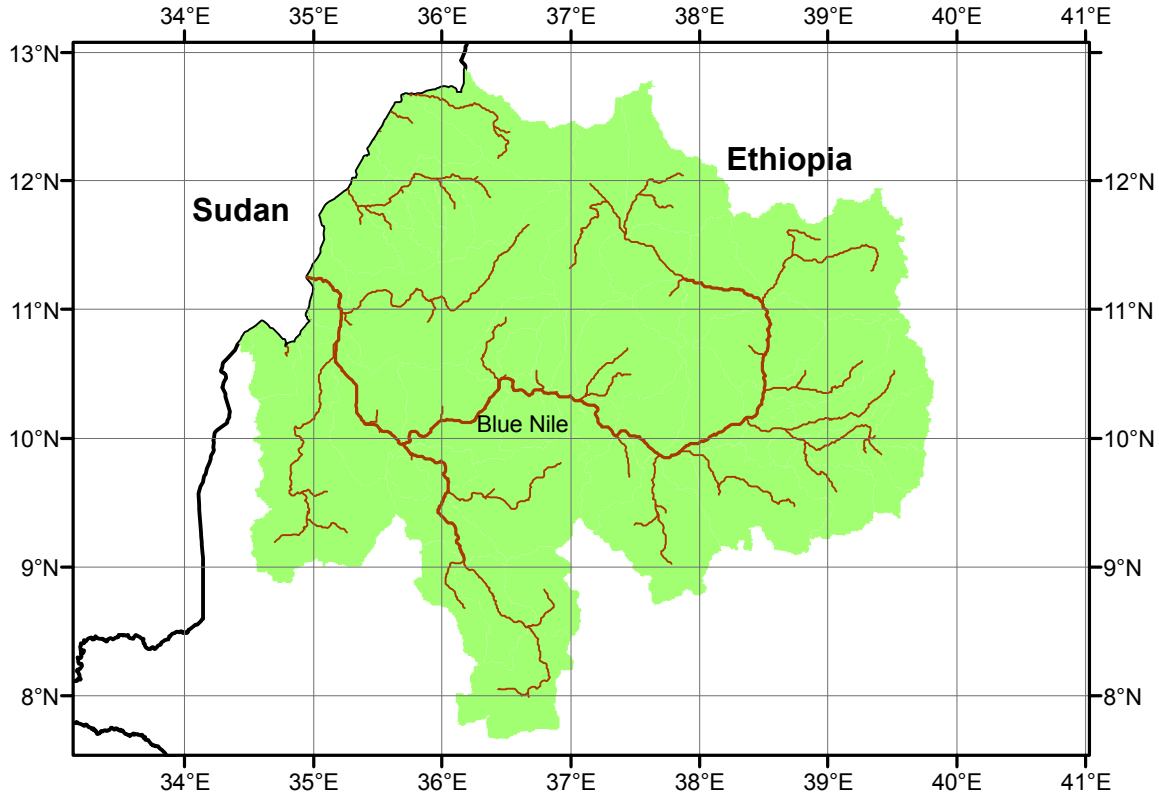

Figure 1: The Upper Blue Nile Basin, Ethiopia

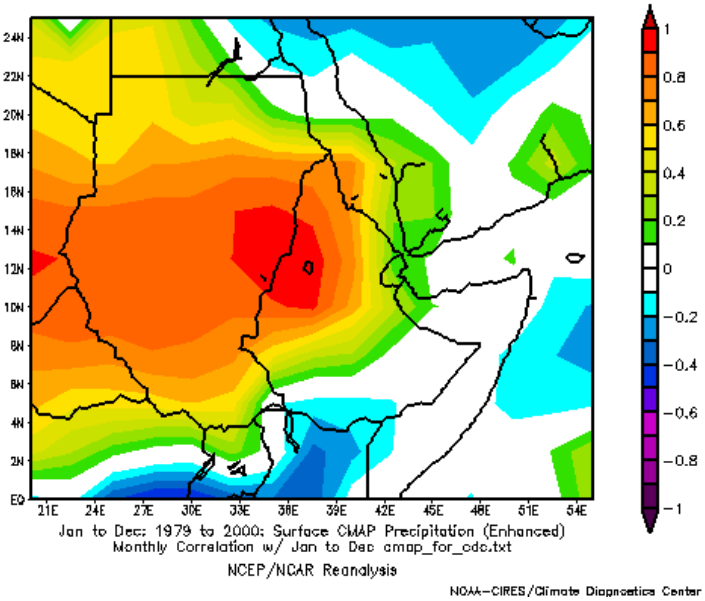

Figure 2: Correlation of CRU and CMAP precipitation data

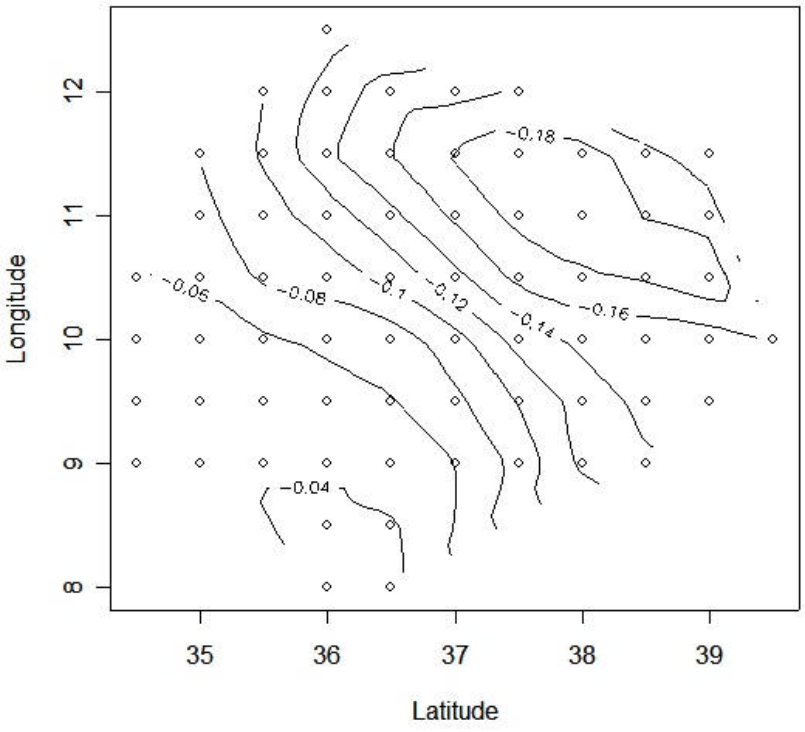

Figure 3: Contours of the first empirical orthogonal function of *Kiremt* precipitation data

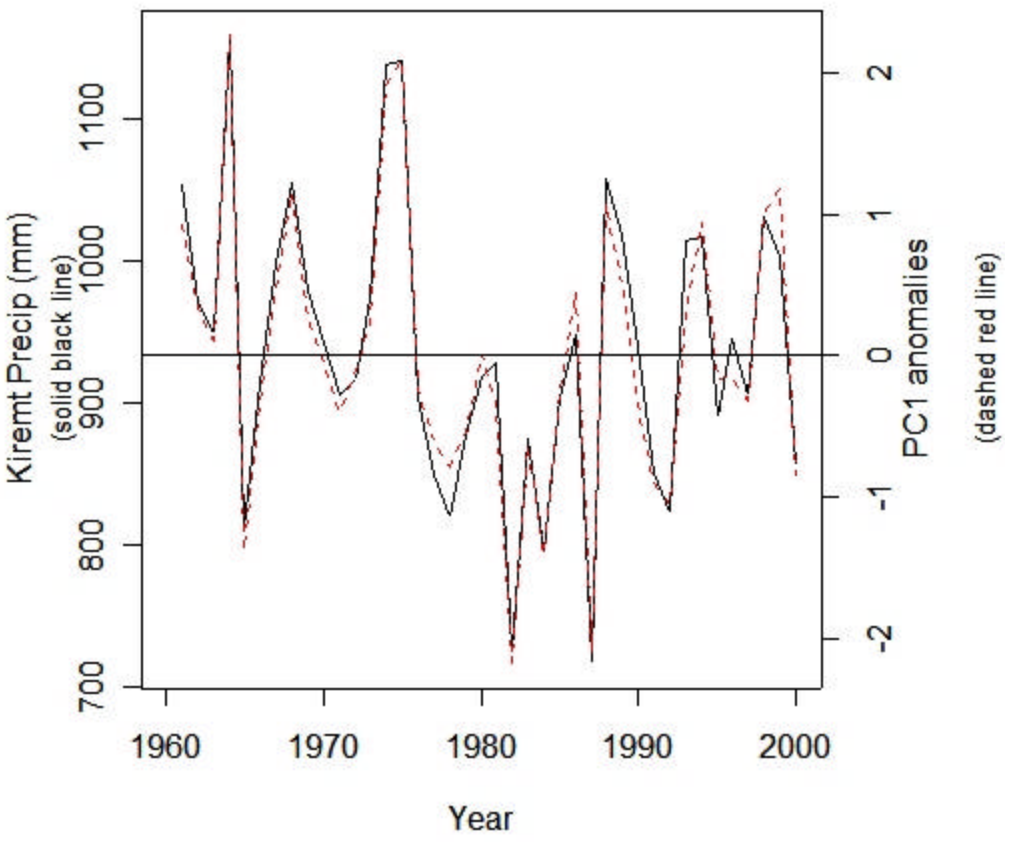

Figure 4: *Kiremt* season precipitation and PC1 anomaly time-series

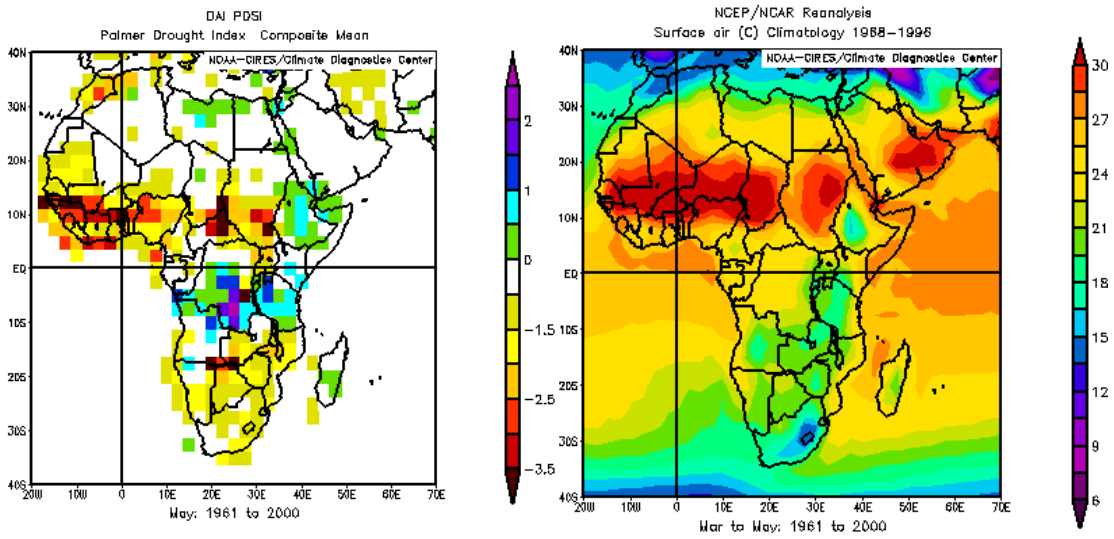

(a) (b)

Figure 5: May Palmer Drought Severity Index (a) and March-May Air Temperature (b)

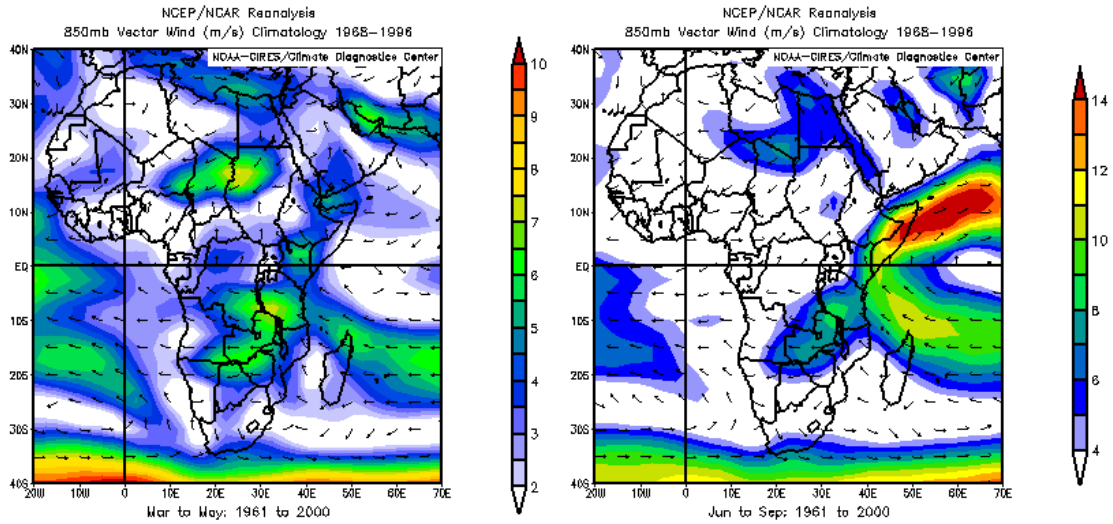

(a) (b)

Figure 6: African wind patterns during the March-May (a) and *Kiremt* (b) seasons

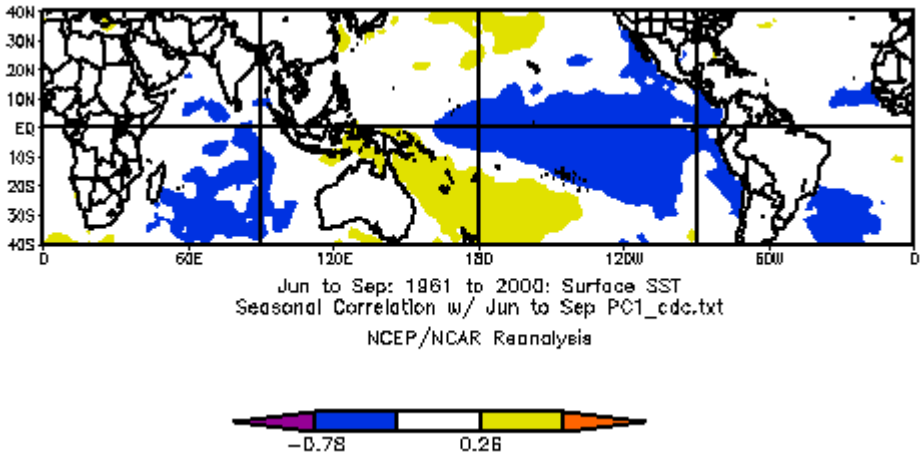

Figure 7: Correlation map of the first principal component of UBN summer precipitation and global sea-surface temperatures (shaded region represents 90% significance level)

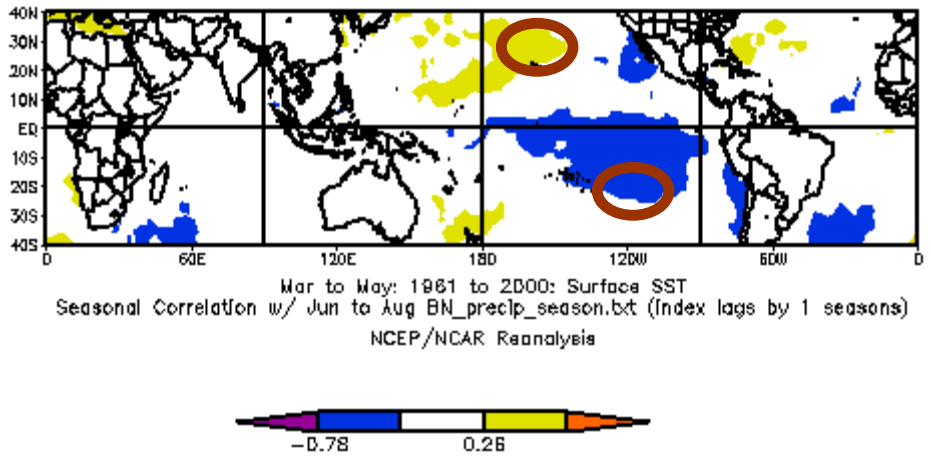

Figure 8: Correlation map of UBN summer precipitation with March-May sea-surface temperatures (R^2=+0.53, R^2=-0.44, Index: R^2=+0.56; shaded regions represent 90% significance level)

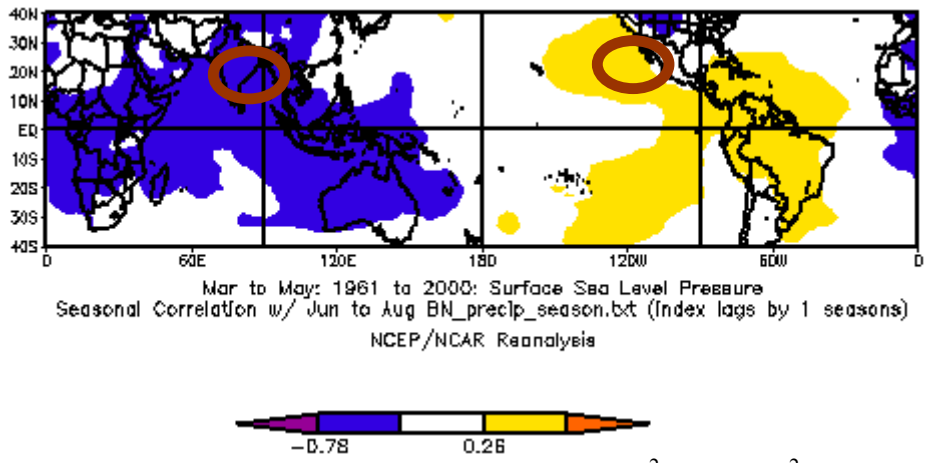

Figure 9: Same as Figure 8 but with sea-level pressures (R^2=+0.57, R^2=-0.52, Index: R^2=+0.60)

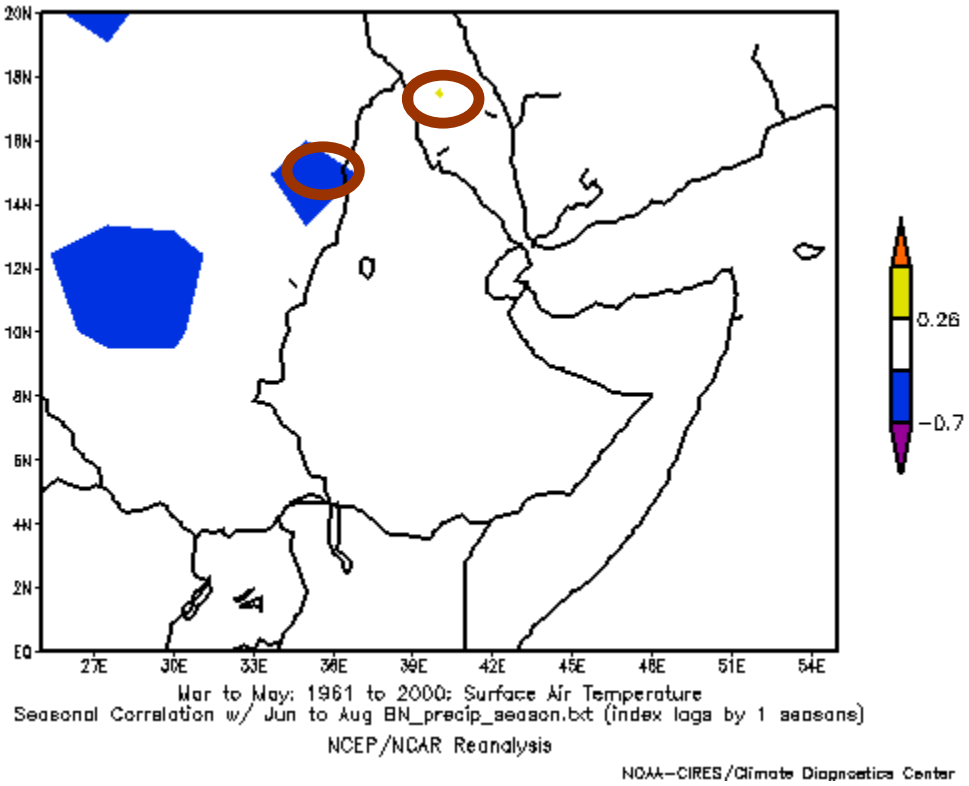

Figure 10: Same as Figure 8 but with air temperature (R^2=+0.14, R^2=-0.29, Index: R^2=+0.45)

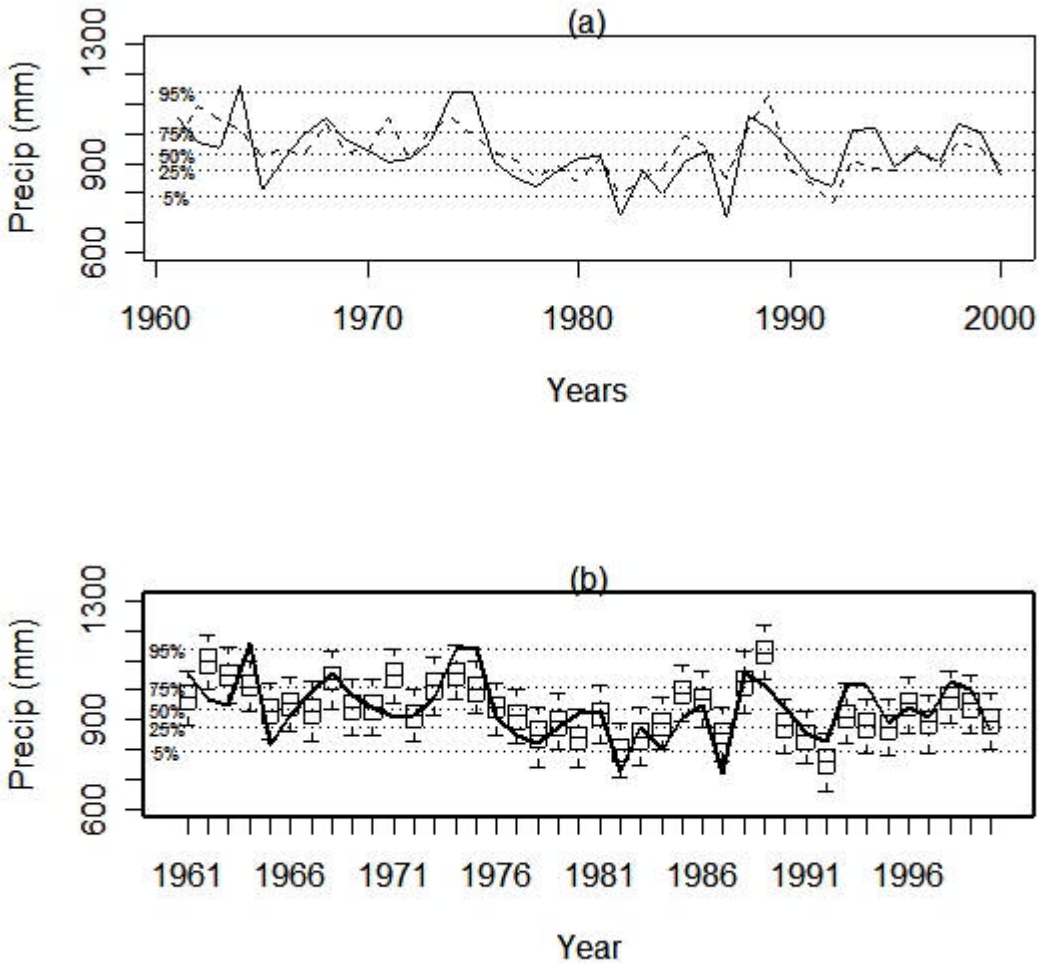

Figure 11: Local polynomial modeling approach forecast results. Observed data shown as solid
line; cross-validated model estimates shown as dashed line and boxes

(a) observed and cross-validated estimates (R^2 = +0.67) with horizontal lines at percentiles from the observed seasonal precipitation

(b) box plots of cross-validated ensembles(RPSS median = 0.39) with horizontal lines at percentiles from the observed seasonal precipitation

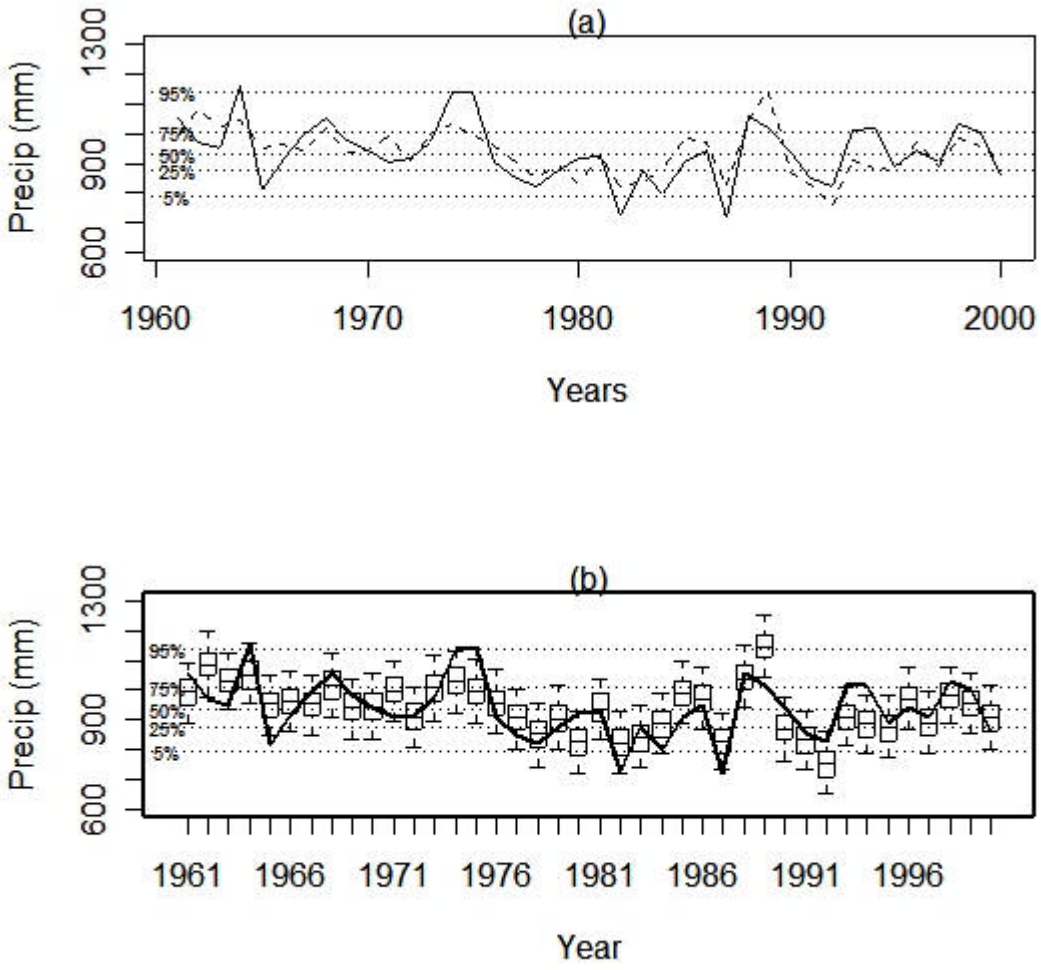

Figure 12: Linear modeling approach forecast results. Observed data shown as solid line; cross-validated model estimates shown as dashed line and boxes

(a) observed and cross-validated estimates (R^2 = +0.69) with horizontal lines at percentiles from the observed seasonal precipitation

(b) box plots of cross-validated ensembles(RPSS median = 0.25) with horizontal lines at percentiles from the observed seasonal precipitation

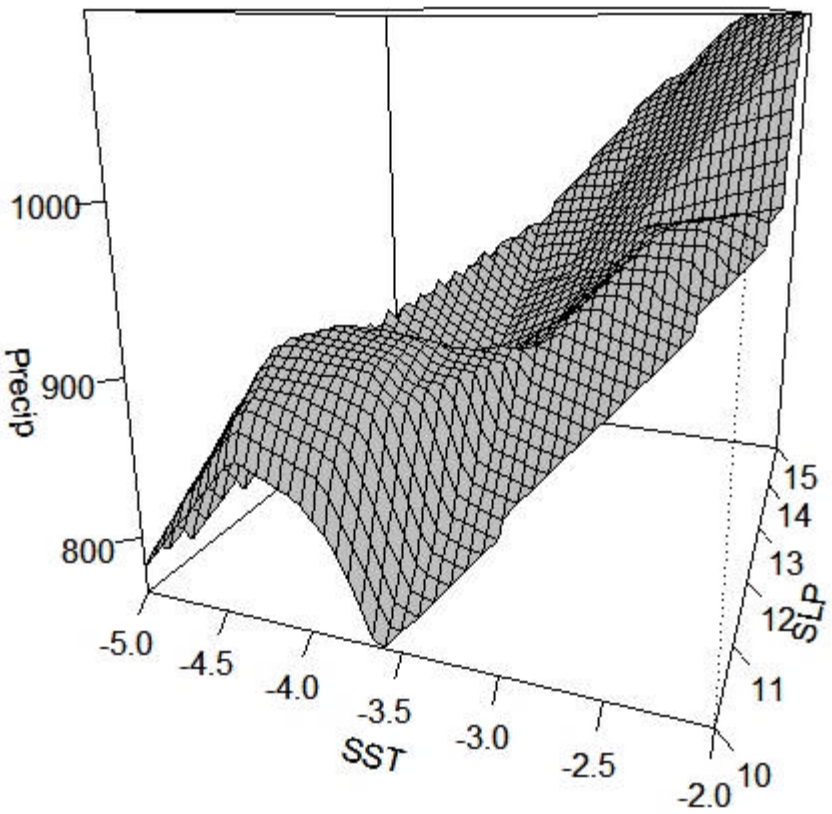

Figure 13: Surface plot of *Kiremt* season precipitation as a function of SST and SLP predictors.

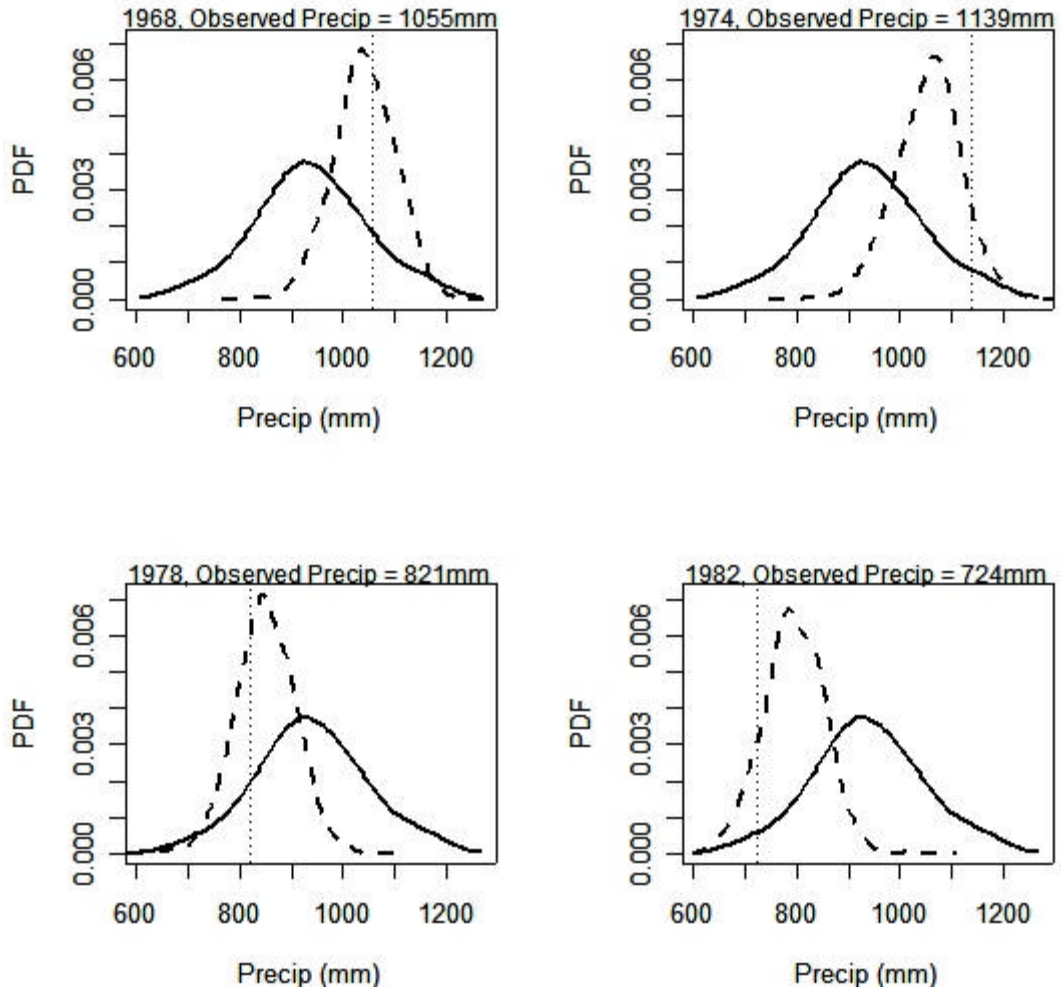

Figure 14: PDF for wet (top) and dry (bottom) years. Climatological PDF shown as solid line; ensemble forecast PDF shown as dashed line. The observed precipitation is shown as a dotted vertical line.

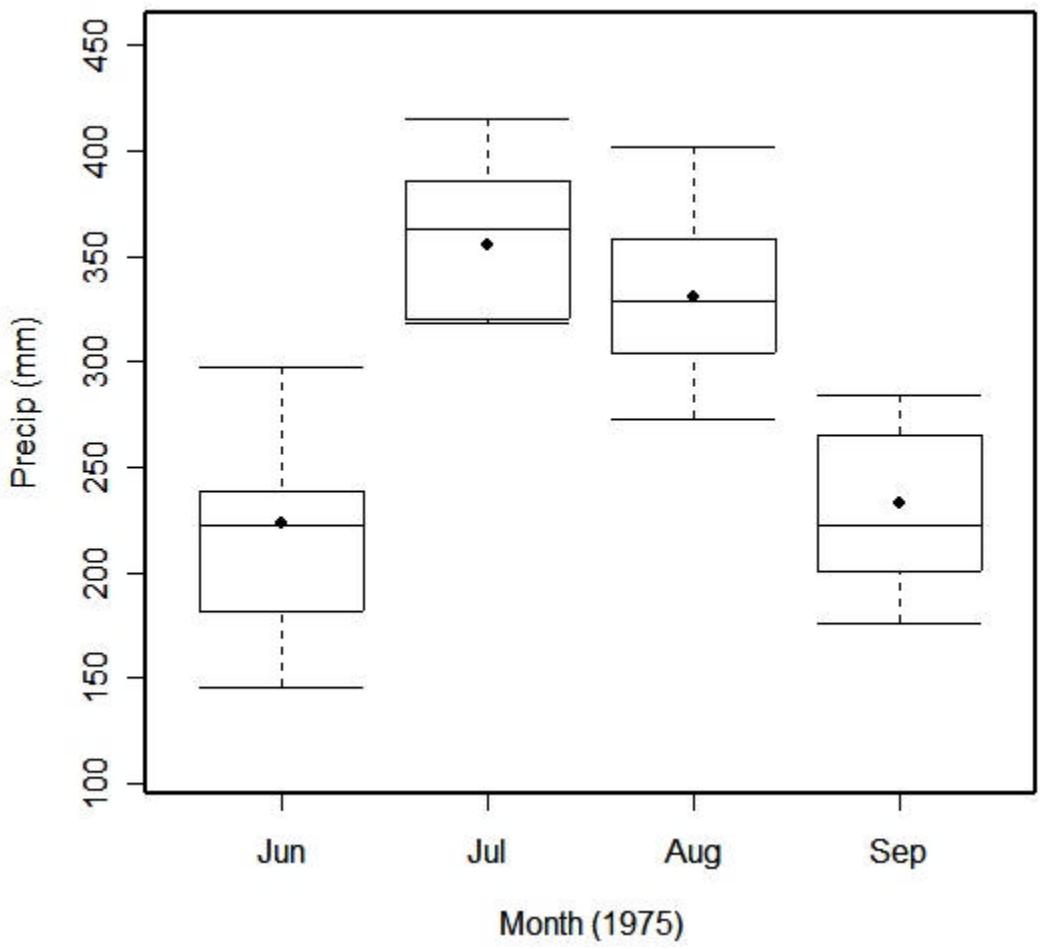

Figure 15: Box plots of disaggregated monthly forecasts of *Kiremt* seasonal ensemble forecast for 1975

Table Captions

Table 1: Correlation of *Kiremt* season precipitation and ENSO climate indices for varying sets of leading months; bold values are statistically significant at the 90% level ($\pm$ 0.26)

Table 2: Potential large-scale predictors of *Kiremt* season precipitation; bold represent optimal set

Table 3: Exceedance and non-exceedance probabilities for forecasting wet and dry years

Tables

Table 1: Correlation of *Kiremt* season precipitation and ENSO climate indices for varying sets of leading months; bold values are statistically significant at the 90% level (± 0.26)

Index	*JFM*	*FMA*	*MAM*
Niño 1+2	-0.19	-0.23	-0.25
Niño 3	-0.19	**-0.33**	**-0.39**
SOI	0.22	**0.29**	**0.38**

Table 2: Potential large-scale predictors of *Kiremt* season precipitation; bold represent optimal set

Potential Predictor	*Region*		*Correlation Value*
Sea-level pressure	20.0 - 27.5N,	122.5 - 130W	+ 0.57
Sea-level pressure	20.0 - 22.5N,	80.0 - 85.0E	- 0.51
Sea-level pressure index			+ 0.60
Sea-surface temperature	25.7N,	155.6 - 157.5W	+ 0.53
Sea-surface temperature	16.2 – 20.0S,	110.5 – 120.0W	- 0.44
Sea-surface temperature index			+ 0.56
Geopotential height (500mb)	30.0 – 35.0S,	10.0 – 25.0W	- 0.48
Outgoing long-wave radiation	1.0 – 4.8S,	48.8 – 52.5E	- 0.56
Air temperature	17.5N,	37.5 – 40.0E	+ 0.14
Air temperature	15.0N,	32.5 – 35.0E	- 0.29
Air temperature index			+ 0.45
Palmer Drought Severity Index	13.75-16.25N,	41.25-43.75E	+ 0.33

Table 3: Exceedance and non-exceedance probabilities for forecasting wet and dry years

Year	Climatology	Linear Approach	Local Polynomial Approach
	Exceedance (wet) / Non-exceedance (dry) Probability, %		
1964(wet)	10.0	39.0	21.0
1968 (wet)	10.0	25.8	34.3
1974 (wet)	10.0	32.6	42.5
1987 (dry)	10.0	42.9	25.2
1978 (dry)	10.0	32.2	30.1
1982 (dry)	10.0	40.8	57.9